

Seasonal variation of leaf area index (LAI) over paddy rice fields in NE China: Intercomparison of destructive sampling, LAI-2200, digital hemispherical photography (DHP), and AccuPAR methods

Hongliang Fang^{a,*}, Wenjuan Li^{a,b}, Shanshan Wei^{a,b}, Chongya Jiang^{a,b}

^a LREIS, Institute of Geographic Sciences and Natural Resources Research, Chinese Academy of Sciences, Beijing 100101, China

^b University of Chinese Academy of Sciences, Beijing 100049, China

ARTICLE INFO

Article history:

Received 24 February 2014

Received in revised form 19 July 2014

Accepted 7 August 2014

Keywords:

Leaf area index (LAI)

Plant area index (PAI)

Rice

Destructive sampling

Gap fraction

Clumping index

ABSTRACT

Continuous field leaf area index (LAI) measurement has become increasingly important for the validation of remote sensing LAI products. A seasonal field campaign was carried out to take continuous LAI measurements over paddy rice fields in NE China in 2012. Three indirect optical methods, LAI-2200, digital hemispherical photography (DHP), and AccuPAR, were compared with a destructive sampling method conducted concurrently. Corrections for the clumping effect were applied to the effective plant area indices (PAI_{eff}) estimated from the indirect optical measurements.

Both LAI-2200 and DHP produce consistent PAI_{eff} estimates over the season ($R^2 = 0.76$, $\text{RMSE} = 0.97$). The clumping index (CI) values obtained from DHP generally decrease with plant growth and range between 0.63 and 0.74 during the peak growing period from day of year (DOY) 191–230. The CI values retrieved from DHP photos generally decrease with increasing view angles. The optical PAI and LAI values estimated from LAI-2200 and DHP correspond very well with the destructive values before DOY 230 ($R^2 = 0.75$, $\text{RMSE} = 1.15$ for PAI and $R^2 = 0.78$, $\text{RMSE} = 0.74$ for LAI), and the relative errors are less than 10% and 5%, respectively, for the two instruments. Omitting ring 5 for LAI-2200 generates very accurate PAI and LAI estimations during the peak season. Nevertheless, AccuPAR underestimates the PAI_{eff} , PAI, and LAI values obtained from other methods (up to 30%). After DOY 231, the capability to detect PAI decreases significantly for both destructive and optical methods due to the leaf senescence and the DHP classification difficulty. In general, rice PAI could be accurately estimated with LAI-2200 and DHP before senescence if the clumping effect could be properly taken into account. The seasonal continuous LAI measurements obtained from this study are valuable for the validation of remote sensing LAI products.

© 2014 Elsevier B.V. All rights reserved.

1. Introduction

Leaf area index (LAI) corresponds to one half the total green leaf area per unit horizontal ground surface area (GCOS, 2011). It is one of the essential climate variables identified by the Global Climate Observing System (GCOS) and has been applied in a range of ecological, hydrological, and biogeochemical models as a primary ecological and biophysical parameter (GCOS, 2011). Over the last decade, a number of global LAI products with different spatial and temporal characteristics have become available (Fang et al., 2013). To properly use the products in various models, it is critical to understand and quantify the uncertainties associated with

the LAI products (Gobron and Verstraete, 2009; Lafont et al., 2012; Morisette et al., 2006).

Reliable and consistent field LAI estimates are indispensable for LAI product development and validation and for the application communities. Field LAI can be estimated using either direct sampling or indirect optical methods (Fang et al., 2012b; Garrigues et al., 2008; Jonckheere et al., 2004; Weiss et al., 2004). With the direct sampling method, LAI can be assessed by destructively harvesting leaves and measuring their area in the field or in the laboratory. LAI values obtained from the destructive sampling method are considered accurate and are often used as references for the indirect optical estimates. However, the destructive method is labor and time consuming and is difficult to deploy over large areas and for repeated measurements. The indirect optical methods derive LAI through measurements of canopy gap fraction or transmittance. The LAI-2200 and LAI-2000 Plant Canopy Analyzers (PCA), digital hemispheric photography (DHP), TRAC, and AccuPAR are some

* Corresponding author. Tel.: +86 10 64888005; fax: +86 10 64889630.

E-mail address: fanghl@lreis.ac.cn (H. Fang).

common instruments for indirect LAI estimation. The indirect optical methods are non-destructive and cost-effective. However, they are sensitive to the presence of plant elements other than green leaves (e.g., branches, trunks, and senescent leaves) and are subject to theoretical assumptions (e.g., the black leaves for LAI-2200) and arbitrary thresholds (e.g., the DHP method).

Paddy rice fields are dominant in the agricultural areas in Asian countries. Accurate estimation of rice LAI is one of the most important objectives in LAI product validation. Nevertheless, field LAI measurements and validation studies are seriously deficient for paddy rice fields because of the complexity of this ecosystem. First, the uncertainties in existing optical measurements are usually unknown because of the diverse measurement schemes and environments. Therefore, destructive methods are necessary to assess the accuracies of the optical methods. However, the destructive data have been lacking for most validation datasets even though they are critical to properly validate remote sensing LAI products (Leblanc et al., 2005). Second, green and senescent leaves must be separated in the destructive sampling procedure because by definition LAI represents only the green leaves, and the yellow leaves are not photosynthetically active. Third, stems may represent a very significant part of the total plant area index (PAI), and the stem area index (SAI) is an important physiological parameter in land surface models (Bonan and Levis, 2006; Tian et al., 2004). Therefore, it is mandatory to consider all the green elements, including stems and leaves, when observing paddy rice. Finally, more and more studies have focused on the validation of the LAI time series products (Camacho et al., 2013; Claverie et al., 2013; Fang et al., 2012a; Heiskanen et al., 2012; Xiao et al., 2014). It is therefore imperative to obtain temporally continuous measurements for rice LAI validation.

The objective of this study is to assess the performance of different field LAI estimation methods for the rice ecosystem. This study extends and contributes to current instrument comparison studies in several aspects. First, continuous seasonal field measurements were carried out in a large and homogeneous rice planting area in NE China. Second, as the main goal, LAI estimates from different optical instruments (LAI-2200, DHP, and AccuPAR) were compared with the destructive sampling results. The field measurements were performed following the Committee on Earth Observation Satellites (CEOS) elementary sampling units (ESU) protocol (Morisette et al., 2006). Third, in addition to LAI, the canopy gap fraction and clumping index were also retrieved and compared in the study. Last but not least, a seasonally continuous field LAI database was constructed for further validation and modeling studies. This study addresses several crucial questions: (1) how do the indirect optical methods perform compared to the destructive LAI at the landscape level? (2) How do the canopy structural variables evolve across the seasons? and (3) what are the potential uncertainties in field LAI measurements and how can they be minimized?

2. Methods

2.1. Study area and ground sampling design

The study area is located at the Honghe Farm ($47^{\circ}39'N$, $133^{\circ}31'E$) in the Heilongjiang province, NE China (Fig. 1). The area has a typical temperate humid continental monsoon climate, with long cold winter and warm humid summer. The monthly mean temperature ranges from $-20^{\circ}C$ in January to about $22^{\circ}C$ in July, with a mean annual temperature of $2.52^{\circ}C$. The mean annual precipitation is approximately 558 mm, with substantial interannual and seasonal variation (Song et al., 2009). The main soil type is the albic bleached meadow soil (Albaqualfs) (Yang et al., 2013). The water and soil in the field are completely frozen from late October to April and begin to thaw in late April.

The paddy rice fields are flat, with more than 5 km homogeneity and rectangular fields approximately $30\text{ m} \times 100\text{ m}$ in size. The rice-cropping practices are similar in the region, growing one crop per year during the summer season (May–September). A single rice variety (*Japonica*) is grown and is normally transplanted in late May. The dates for the flowering, grain filling, and maturity stages are early July, early August, and early September, respectively. The soil surface is in flooded conditions during most of the growing periods.

Ground LAI measurements were continuously carried out from June 11 (day of year (DOY) 163) to September 17, 2012 (DOY 261), from shortly after the rice turned green to when all rice was ready for harvest. The field campaign was part of a multi-year Paddy Rice Experiment in the Sanjiang Plain (PRESP), which was established to validate land products generated by remote sensors over paddy rice fields (Fang et al., 2014). Five plots (A–E), four at the four corners and one at the center, were chosen for intensive ground based measurements (Fig. 1). Each plot was planted with a cultivar type and managed individually. Approximately 50–60 Elementary Sampling Units (ESUs) $15 \times 15\text{ m}^2$ or $20 \times 20\text{ m}^2$ in size were selected within each plot. ESUs were located at least 1.5 m away from the field borders. ESU-level sampling was performed along a diamond shaped box with two 15-m diagonals as recommended by the VALERI network (<http://w3.avignon.inra.fr/valeri/>).

To reduce the impact of destructive sampling and measurement disturbance, a moving sampling strategy was used. Four ESUs within a plot were selected in the first week, and LAI measurements were taken using one direct or indirect method for each ESU. According to the moving sampling strategy, the group of used ESUs was discarded, and another four parallel ESUs were selected for the next week. Major morphological changes and field conditions were observed and recorded. More details about the field work can be found in Fang et al. (2014).

2.2. Field measurement methods

Field measurements were performed sequentially for the five plots every week to capture the canopy structural dynamics. All instruments were newly procured and factory calibrated. All optical measurements were conducted near sunset or under overcast conditions because the parameter sensitivity and the retrieval errors increase under direct illuminations (Demarez et al., 2008; Garrigues et al., 2008).

2.2.1. LAI-2200 plant canopy analyzer

An LAI-2200 Plant Canopy Analyzer (PCA) (LI-COR Inc., Lincoln, Nebraska) was used to estimate the rice PAI because all parts of the plants, including green leaves, yellow leaves, stems, and seeds contribute to the canopy transmittance process. Following the instruction manual for row crops, ground measurements were made along diagonal transects between the rows (Fang et al., 2014). Two repeats were made for each measurement, with one above canopy and four below canopy readings. For below canopy measurements, the instrument was held about 5 cm above the background soil or shallow water. A 270° view cap was used to shield the sensor from the operator. All PAI values obtained within an ESU were averaged to obtain the ESU PAI.

The average probability of light penetration into the canopy at direction θ is computed as:

$$\overline{P_0(\theta)} = \frac{1}{N} \sum_{j=1}^N \frac{B_j}{A_j} \quad (1)$$

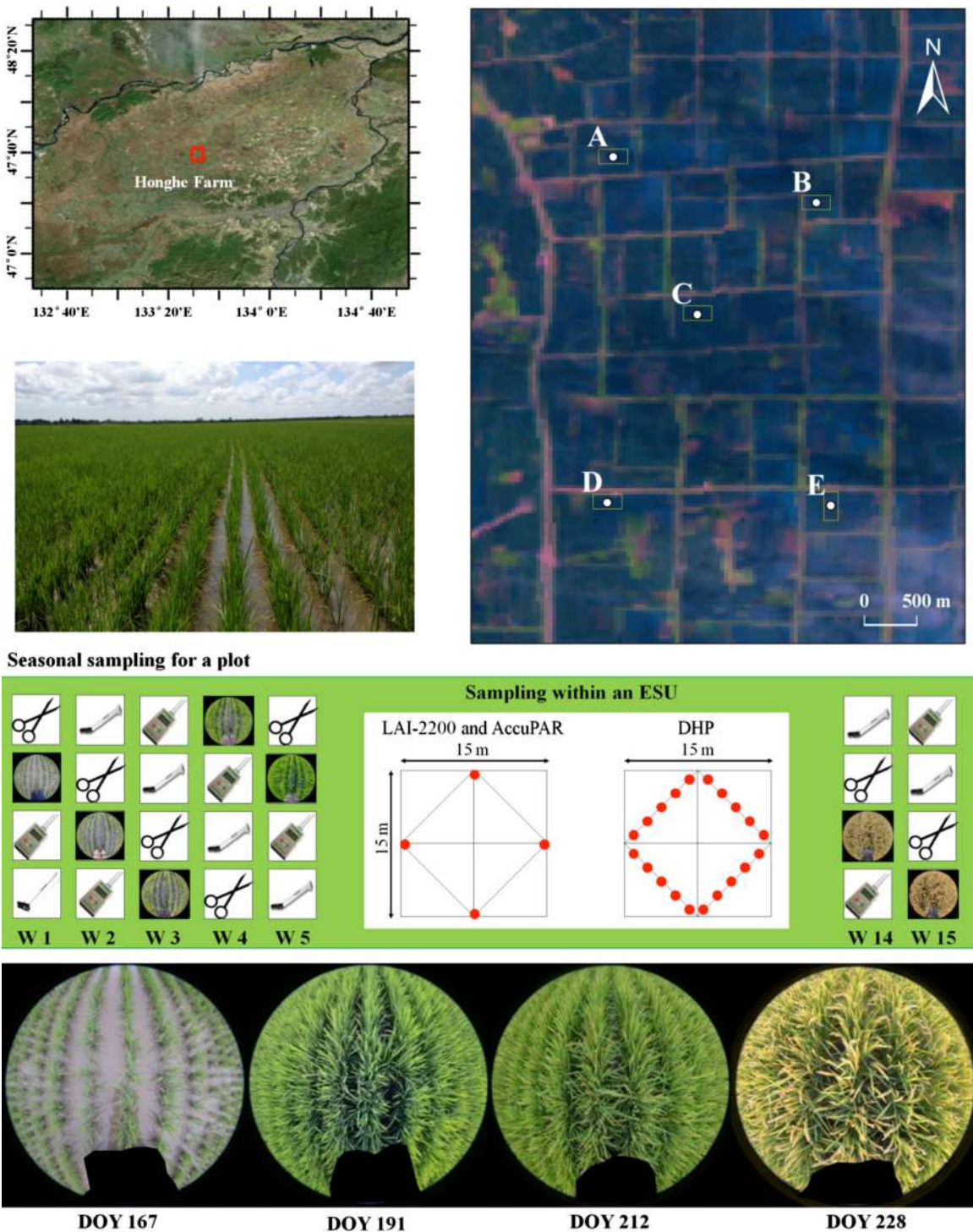


Fig. 1. Location of the study area in the Sanjiang Plain, NE China. The upper panel shows the study area at the Bing Maps™, the locations of the five plots in a Landsat ETM+ image (Jun 3, 2012), and a picture at Plot E (Jun 28, 2013). The middle panel shows the moving sampling strategy within a plot and the optical sampling scheme within an ESU. The four parallel field measurement icons are in the order of destructive, DHP, AccuPAR, and LAI-2200, respectively, for week one (W1). The lower panel shows sample DHP images on DOY 167 (Jun 15), 191 (Jul 9), 212 (Jul 30), and 228 (Aug 15), respectively.

where the subscript j refers to the number of observational pairs ($j = 1 \dots N$) and B_j and A_j are the j th below canopy and above canopy readings, respectively. The gap fraction in direction θ is computed as:

$$P(\theta) = e^{(\overline{\ln P_o(\theta)})} = e^{-\frac{1}{N} \sum_{j=1}^N \ln(B_j/A_j)} \quad (2)$$

Assuming that the foliage elements are randomly distributed in space, the effective PAI (PAI_{eff}) can be estimated by the transmittance in different view angles based on the Miller's formula (Miller, 1967).

$$PAI_{eff} = 2 \int_0^{\pi/2} -\ln P_o(\theta) \cos \theta \sin \theta d\theta \quad (3)$$

For LAI-2200, five concentric conical rings (7° , 23° , 38° , 53° , and 68°) are used to record the incident light. Since multiple observations of $P_o(\theta)$ are available, the PAI_{eff} is calculated as:

$$\text{PAI}_{\text{eff}} = 2 \int_0^{\pi/2} -\overline{\ln P_o(\theta)} \cos \theta \sin \theta d\theta = 2 \sum_{i=1}^5 \bar{K}_i W_i \quad (4)$$

where K_i and W_i are the contact number and the weighting factor, respectively (Appendix A).

To minimize the differences in viewing angles between LAI-2200 (74°) and DHP (60°), the PAI_{eff} was further calculated from LAI-2200 using the first four rings (4R) from Eq. (4). This was also to investigate the effect of excluding the LAI-2200 ring 5, which is usually impacted by diffuse light from multiple scattering (Chen, 1996; Chen et al., 2006). Because the 5-ring (5R) mode is widely used in practice, in this paper, the term LAI-2200 is generally used to represent the 5R results, and the 5R and 4R modes will not be differentiated unless necessary.

2.2.2. Digital hemispherical photography (DHP)

The DHP images were taken using a Nikon D5100 camera and a 4.5 mm F2.8 EX DC circular fisheye converter. An ultraviolet cap was used to protect the lens from dust and rain. The total height of the camera and the lens was about 16.5 cm. Two bubble levels were attached to the camera to keep it horizontal for both downward and upward viewing directions. The fisheye camera was calibrated before the experiment using the method described in the CAN_EYE manual (version 6.3.3) (Weiss and Baret, 2010).

Downward-looking photos were taken before July 10 (DOY 192), when the rice entered the flowering stage. The distance between the camera and the top canopy was set to about 0.8–1.5 m to avoid having individual leaves too close to the camera.

When the rice grew higher than 70 cm (after July 10), upward-looking photos were taken together with the downward measurements at the same location. For the upward measurements, the camera was placed right above the ground soil or water. Before July 26 (DOY 208), the camera was set to automatic exposure to avoid the saturation issues during the downward measurement (Demarez et al., 2008). After that, the aperture and shutter speed of the camera were manually adjusted to avoid overexposure because the sunlight intensity could change considerably during the shift from downward to upward measurements. During the first 10 days, the downward photos were randomly taken with azimuthally varying directions. After that, all DHP photos were taken with a fixed azimuth angle to the row direction to examine the impact of viewing angle on the CI calculation (Weiss et al., 2004). The photos were stored in the JPEG format at a resolution of 3264×4928 pixels. All valid photos (8–20) over one ESU were processed simultaneously by the CAN_EYE software (version 6.3.3) to extract the structural variables (Weiss and Baret, 2010). The valid range of fisheye images was limited to 60° zenith angle to avoid edge distortions. The angular resolutions for zenith and azimuth directions were set to 10° .

A thresholding process is necessary to separate the foliage from the soil background (downward view) or the sky (upward view). To minimize subjective errors, one operator performed the entire thresholding and classification procedures. PAI_{eff} is retrieved in CAN_EYE using lookup-table techniques and assuming an ellipsoidal distribution of the leaf inclination (Weiss et al., 2000). A large range of random combinations of LAI (0–10) and LAD (10° – 80°) values are used to build a database of the relationship between $P_o(\theta)$ and PAI_{eff} following the Beer-Lambert's law (Nilson, 1971):

$$P_o(\theta) = e^{-G(\theta) \cdot \text{PAI}_{\text{eff}} / \cos(\theta)} \quad (5)$$

where $G(\theta)$ is the projection function. In this study, the PAI_{eff} was also calculated from DHP using the Miller's equations (Eq. (3)) to compare with the LAI-2200 4R results from Eq. (4).

The clumping index (CI) in direction θ is computed for each ESU using the logarithm gap fraction averaging method (Lang and Xiang, 1986):

$$\text{CI}(\theta) = \frac{\ln \overline{P_o(\theta)}}{\ln P_o(\theta)} \quad (6)$$

The optical PAI can be computed by:

$$\text{PAI} = \frac{\text{PAI}_{\text{eff}}}{\text{CI}} \quad (7)$$

where CI is the average clumping index over all zenith angles.

2.2.3. AccuPAR ceptometer

Decagon's AccuPAR model LP-80 PAR/LAI ceptometer measures photosynthetically absorbed radiation (PAR) using 80 individual sensors (field of view: 180°) on its probe. It measures radiation by locating the probe beneath the canopy and above the canopy and then computes PAI based on angularly integrated transmittance. Before measurement, the instrument was calibrated according to the instruction manual. The AccuPAR was placed at about 45° to the row direction to minimize the row effects on LAI readings. PAI_{eff} is derived following the equations to predict the scattered and transmitted PAR (Norman and Welles, 1983):

$$\text{PAI}_{\text{eff}} = \frac{[(1 - (1/2k)f_b) - 1] \ln \tau}{A(1 - 0.47f_b)} \quad (8)$$

where τ is the transmission coefficient obtained from the ratio of the below canopy and above canopy PARs, f_b is the fraction of the incident beam PAR, and A is a function of the leaf absorptivity in the PAR band. The parameter k is the extinction coefficient for the canopy and is a function of solar zenith angle (SZA) and leaf angular distribution (LAD). Details about the parameters can be found in the AccuPAR manual (Decagon Devices, 2004).

2.2.4. Destructive sampling measurement

Within each ESU, five bundles were randomly harvested at water level, placed in a sealed plastic bag or on ice when the plants were too long, and taken to the laboratory inside a cooler box. Ex situ measurements were taken immediately after returning the samples to the laboratory. Green leaves were separated from yellow leaves, stems, and ear components. If a larger proportion of a leaf was green (yellow), it was recognized as a green (yellow) leaf. The areas of leaves, young stems, and ears were measured with a leaf area meter (model LI-3100C, LI-COR: Lincoln, Nebraska, U.S.). After June 19 (DOY 171), the rice stems were deemed too thick for the area meter and were measured with a CanoScan LiDE 110 laser scanner. The areas of seeds were measured using both the LI-3100C and the scanner. The rice tissues were put on a white paper and scanned at 300 dpi resolution. The scanned images were processed by a thresholding code to separate the rice parts from the white background. For all non-flat elements (stems, ears, and rolled leaves), the projected area was estimated in a way similar to the indirect optical observations (Chen and Black, 1992; Deblonde et al., 1994; Lang, 1987). Other studies have considered the developed surface area (Baret et al., 2010; Lang et al., 1991; Stenberg, 2006). However, it is difficult to extend and measure the flat surface area of rolled senescent leaves. Therefore, the surface area measurement was not considered in this study. If stems were treated as cylinders, the ratio of half the total surface area of the convex hull to the projected area would be $\pi/2$, i.e., 1.57 (Chen and Cihlar, 1995; Lang, 1991).

The distances between rows and plants were measured five times randomly within an ESU. PAI was calculated as the leaf area per bundle divided by the ground area occupied per bundle. In a similar manner, LAI, yellow leaf area index (YAI), stem area index

(SAI), and PAI were all calculated based on the field measurements. By definition, the clumping index can be calculated as:

$$CI = \frac{PAI_{eff}}{PAI} = \frac{PAI_{eff}(\text{Optical})}{PAI(\text{Destructive})} \quad (9)$$

The optical LAI can be derived from the indirect measurements (Chen, 1996; Chen et al., 2006):

$$LAI = \frac{PAI_{eff}}{CI}(1 - \alpha)(1 - \gamma) \quad (10)$$

where α is the stem-to-total plant area ratio (SAI/PAI) and γ is the yellow to total leaf area ratio (YAI/(LAI + YAI)).

3. Results

3.1. Destructively obtained LAI and PAI

The seasonal variation of LAI and PAI obtained from the destructive methods is shown in Fig. 2 and their statistics in Table 1. The five plots follow fairly consistent seasonal phenological stages of LAI changes. LAI increases after transplant until late July, reaches a maximum at around 4.74, and decreases gradually throughout

August (Fig. 2f). Variations in LAI values are relatively small (<1.40) during the maturity stage in September. Differences exist between the plots in various stages of the growing season. Plot D has the largest peak LAI, reaching 6.65 on DOY 202 (July 20), followed by plots A and E, whereas plots B and C have the smallest peak LAI values, at about 4.40 and 3.85 on DOY 191 (July 9) and 194 (July 12), respectively.

Yellow leaves represent a small portion (<5%) of the LAI before DOY 230, but quickly reach about 35% near the harvest time. The average YAI varies around 0.57 between DOY 231 and 261 and the yellow-to-green leaf area ratio is about 0.36 during this period (Table 1). The highest YAI is observed at plot D (1.11) on DOY 254 (September 10), when the yellow-to-green leaf ratio is about 50.5% on this day (Fig. 2d).

The total PAI shows a fairly similar seasonal change to that of LAI (Fig. 2). The PAI values obtained by the scanner are slightly less (~0.06 on average) than those estimated by the LI-3100C over the entire growing season. However, this difference is statistically insignificant (Student's *t*-test, $p > 0.40$) and is mainly attributed to crop residuals left on the LI-3100C transfer tape. Therefore, the PAI obtained by the scanner was considered as the destructive PAI in this study. On average, PAI approaches a maximum value

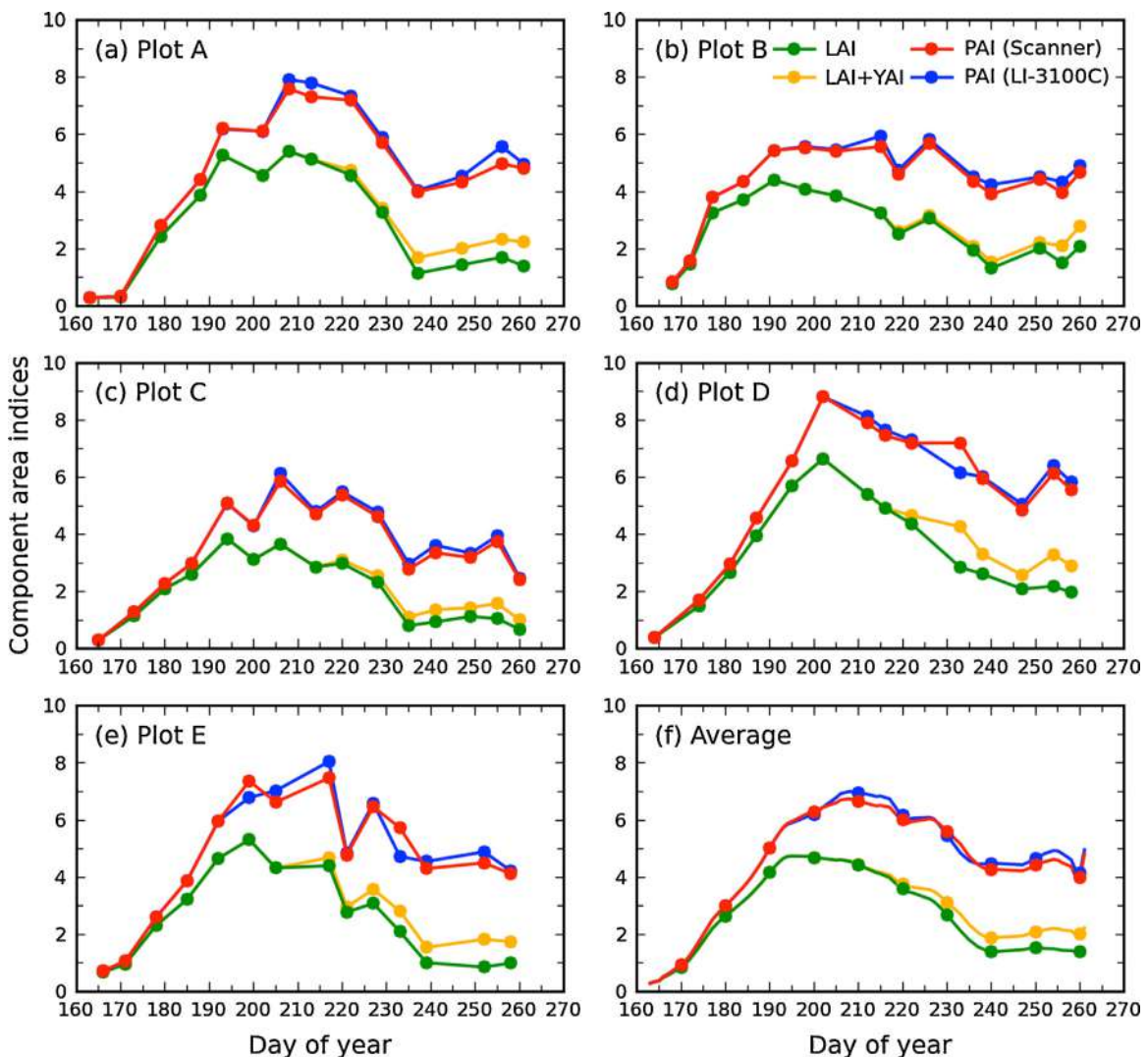


Fig. 2. Seasonal variation of leaf and plant area indices obtained from the destructive method in 2012. Panels (a)–(e) are for plots A–E, respectively. Panel (f) shows the average of all plots. The green lines show the green leaf area index (LAI) and the yellow lines are for the sum of LAI and the yellow area index (YAI). The blue and red lines show the PAIs obtained from LI-3100C and the scanner, respectively. (For interpretation of the references to color in this figure legend, the reader is referred to the web version of the article.)

Table 1

Rice area indices calculated from the destructive method over different periods of the season. The values in the brackets show the standard deviations. LAI: leaf area index (LAI); YAI: yellow leaf area index; SAI: stem and seed area index; PAI: plant area index (=LAI + YAI + SAI). SAI and PAI values are from the LI-3100C and the scanner measurements, respectively.

DOYs	160–190	191–200	201–230	231–261
LAI	2.04 (1.26)	4.66 (0.13)	3.94 (0.62)	1.58 (0.28)
YAI			0.13 (0.14)	0.57 (0.10)
LAI+YAI	2.04 (1.26)	4.66 (0.13)	4.07 (0.48)	2.15 (0.28)
SAI (LI-3100C)	0.31 (0.25)	1.22 (0.19)	2.40 (0.25)	2.49 (0.18)
SAI (scanner)	0.31 (0.25)	1.27 (0.22)	2.24 (0.21)	2.35 (0.12)
PAI (LI-3100C)	2.35 (1.51)	5.88 (0.29)	6.47 (0.44)	4.64 (0.25)
PAI (scanner)	2.35 (1.51)	5.93 (0.32)	6.31 (0.33)	4.50 (0.35)
YAI/LAI			3.3%	36.1%
LAI/PAI (scanner)	86.8%	78.6%	62.4%	35.1%
SAI/PAI (scanner)	13.2%	21.4%	35.5%	52.2%

(6.75) around DOY 208 (July 26), two weeks after the LAI peak. PAI gradually decreases thereafter, mainly because of the leaf area decrease (Fig. 2f). After DOY 231 (August 18), the PAI values become very stable (~4.50) until the end of the season (Table 1). While the PAI values are phenologically similar for the five plots, plot D shows the maximum PAI value at 8.83 on DOY 202 (July 20). A strong wind occurred on DOY 247 (September 3), which blew down

large areas of rice canopy and greatly affected the measurements afterwards.

The stem areas reach maximum about 20 days after LAI and vary little after the peak time (Fig. 2f). The stem-to-total area ratio is about 0.36 from DOY 201–230 (Table 1). After that, stems contribute to about 52.5% of the total PAI. For plot E, stems account for more than 60% of the total PAI after DOY 240 (August 27) (Fig. 2e).

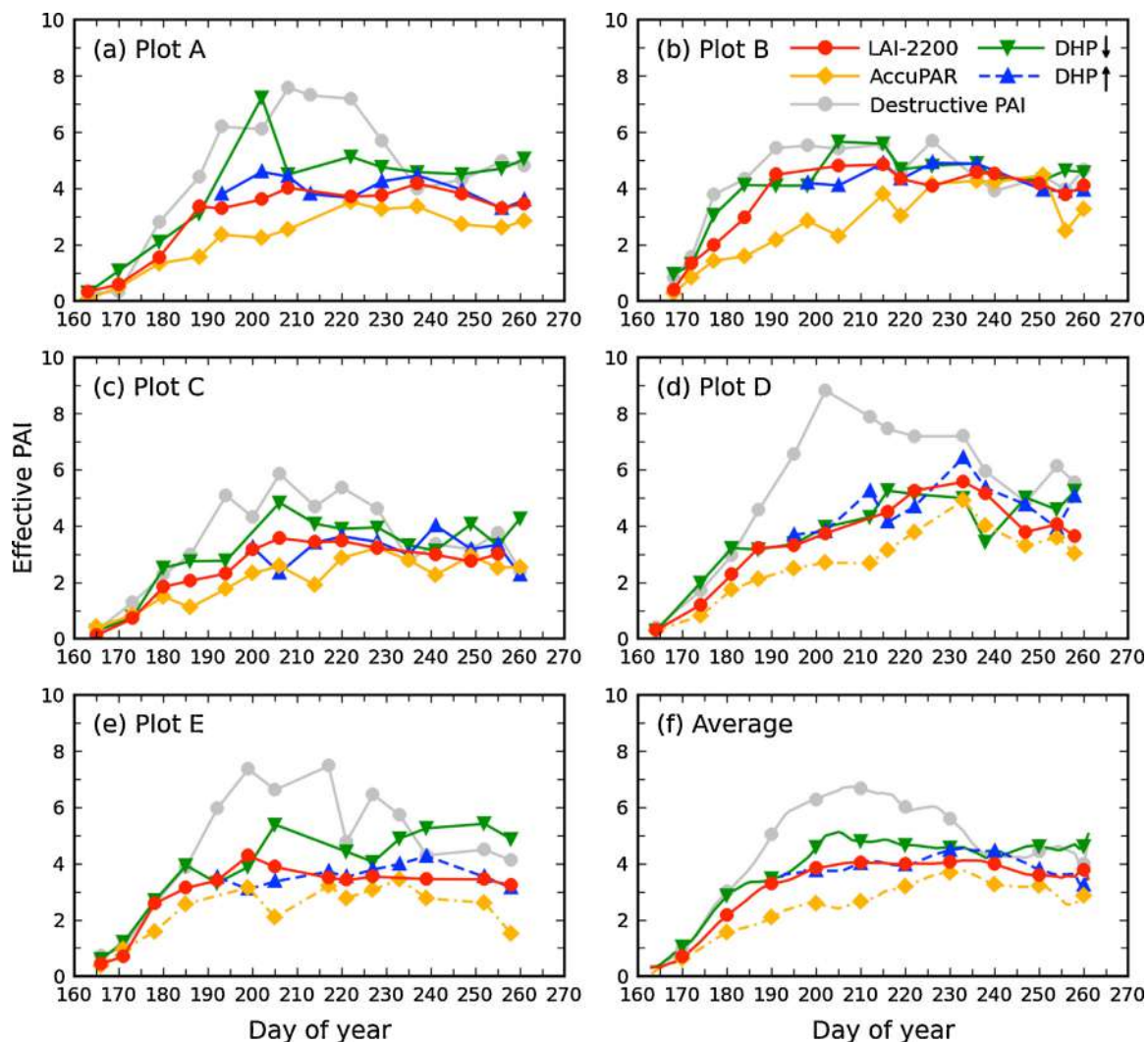


Fig. 3. Seasonal variation of the effective PAI (PAI_{eff}) estimated from LAI-2200, DHP, and AccuPAR for the five plots. Both upward and downward DHP measurements are shown. The destructive PAI (light gray line) obtained from the scanning method (Fig. 2) is shown as a reference. Panels (a)–(e) for plots A–E and panel (f) the average of all plots.

Table 2

Effective plant area index (PAI_{eff}) obtained with the indirect optical methods over different periods of the season. The values in the brackets show the relative differences comparing to the LAI-2200 5R (first row). The last two rows show the average of all LAI-2200 and DHP estimates and the standard deviations.

DOYs	160–190	191–200	201–230	231–261
LAI-2200 5R	1.68	3.57	4.01	3.80
LAI-2200 4R	1.68 (0.0%)	3.72 (4.2%)	4.34 (8.2%) ^{**}	4.11 (8.3%) ^{**}
DHP downward	2.08 (23.8%)	3.95 (10.6%) ^{**}	4.78 (19.2%) ^{**}	4.51 (18.7%) ^{**}
DHP upward		3.70 (3.6%)	4.03 (0.5%)	4.05 (6.6%) [*]
AccuPAR	1.18 (−29.8%) [*]	2.46 (−31.1%) ^{**}	3.00 (−25.2%) ^{**}	3.19 (−16.1%) ^{**}
LAI-2200 5R + DHP	1.88 ± 1.10	3.74 ± 0.29	4.28 ± 0.39	4.12 ± 0.41
LAI-2200 4R + DHP	1.89 ± 1.12	3.80 ± 0.27	4.39 ± 0.35	4.23 ± 0.36

* $p < 0.05$.

** $p < 0.01$.

If the stems were considered as convex hulls, they would account for 75% of the total PAI (Fang et al., 2014).

3.2. Optically derived PAI_{eff}

The seasonal dynamics of PAI_{eff} obtained by LAI-2200, DHP, and AccuPAR for the five plots are depicted in Fig. 3 and their statistics in Table 2. Outlier data due to inclement weather conditions and operator issues were not included in the comparison. PAI_{eff} increases with crop development to a maximum in late July and then decreases slightly (<1.0) until the end of the season. The largest discrepancies (up to 2.7) between the optical instruments are noticed in late July, whereas small deviations (~0.82) appear in mid-August. The downward DHP overestimates LAI-2200 by about 20% between DOY 201 and 230. The upward DHP and LAI-2200 measurements are similar in phase and in magnitude during the season. Both LAI-2200 and DHP measurements show relatively smaller variations after DOY 200 (July 18). AccuPAR underestimates with respect to the other optical instruments over the whole season, especially before DOY 230 (August 17), when the maximum underestimation reaches more than 30% in late July (Fig. 3 and

Table 2). After DOY 231, the difference between AccuPAR and the mean of LAI-2200 and DHP is less than 1.0 (22.6%) (Table 2). In the following text, the mean values of the LAI-2200 and DHP estimates will be considered as the optical PAI_{eff} .

Large variations are observed across the plots at various stages. Several extremely high PAI values are observed for the downward DHP, for example, at plot A (7.24) on DOY 202 (July 20) and plot E (5.40) on DOY 205 (July 23). On the other hand, plot D shows a high PAI value (6.45) for the upward DHP on DOY 233 (August 20). The largest deviations are observed for plot E (Fig. 3). The extreme DHP PAI_{eff} values in plots A and D and the large deviations in plot E are related to uncertainties in the image classification process.

Fig. 4 shows the relationship among the PAI_{eff} values obtained from the optical instruments. The downward DHP and LAI-2200 agree very well ($R^2 = 0.76$, RMSE = 0.97, Fig. 4a) with a small positive bias (~0.61), and the relative errors are less than 20% after DOY 191 (Table 2). Good correspondence can also be observed between the upward DHP and LAI-2200 ($R^2 = 0.50$, RMSE = 0.56, Fig. 4b), with relative errors less than 5% (Table 2). The downward DHP estimates show a positive bias (0.58, 14.5%) over the upward estimates (Fig. 4c). The best relationship is found between LAI-2200

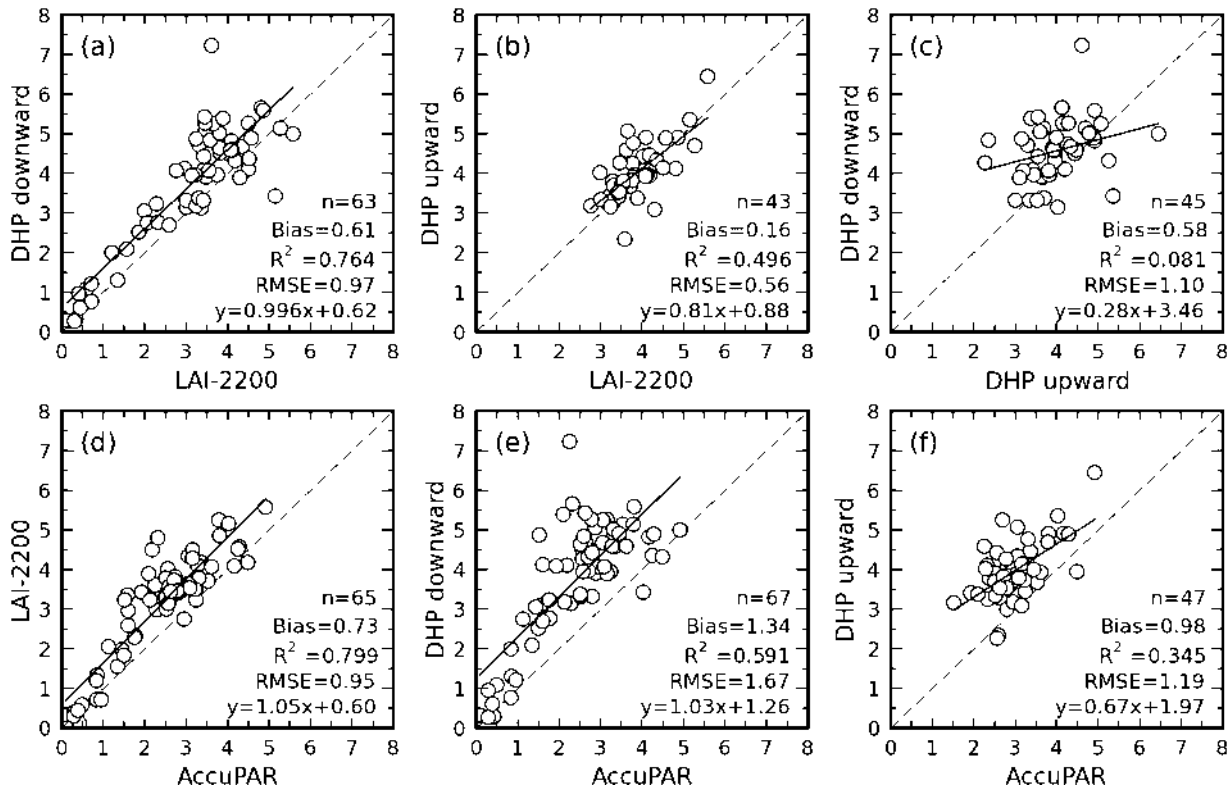


Fig. 4. Comparison of the effective PAIs (PAI_{eff}) estimated from the LAI-2200, DHP, and AccuPAR methods.

Table 3

Comparison of PAI_{eff} values from DHP with the Miller method (Eq. (3)) and LAI-2200 4-ring (4R) and the original DHP LUT method. The values in the brackets show the relative differences comparing to the LAI-2200 4R and to the original DHP results, respectively. The last rows show the average of all LAI-2200 4R and DHP Miller estimates and their standard deviations.

DOYs	160–190	191–200	201–230	231–261
DHP downward Miller	2.10	4.29	5.36	4.52
Vs. LAI-2200 4R	(25.0%)	(15.3%)*	(23.5%)**	(10.0%)**
Vs. DHP downward	(1.0%)	(8.6%)	(12.1%)**	(0.2%)
DHP upward Miller		3.52	3.86	3.83
Vs. LAI-2200 4R		(−5.4%)*	(−11.1%)**	(−6.8%)**
Vs. DHP upward		(−4.9%)**	(−4.2%)**	(−5.4%)*
LAI-2200 4R + DHP Miller	1.89 ± 1.17	3.86 ± 0.44	4.52 ± 0.67	4.15 ± 0.42

* $p < 0.05$.

** $p < 0.01$.

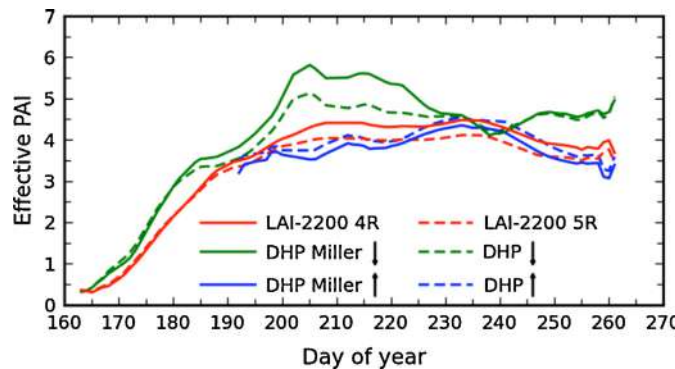


Fig. 5. Seasonal variation of PAI_{eff} estimated from LAI-2200 4-ring (4R) and the DHP Miller methods (Eq. (3)). The original PAI_{eff} retrieved from LAI-2200 5-ring (5R) and the DHP LUT methods are shown in dashed lines.

and AccuPAR ($R^2 = 0.80$, RMSE = 0.95). However, AccuPAR systematically underestimates the LAI-2200 and DHP values (>0.70, or 16%), especially for PAI_{eff} > 1.0.

Fig. 5 shows that the PAI_{eff} values estimated from LAI-2200 5R and 4R are similar before DOY 200 with relative differences less than 5%. When PAI_{eff} is higher than 4.0 after DOY 201, omitting ring 5 results in consistently higher estimates (0.33, 8.2%) than the original 5R results (Table 2). For the downward views, the PAI_{eff} values estimated using the Miller method are larger (<12.0%) than those derived from the original LUT method (Table 3). For the upward DHP, the Miller estimates are slightly smaller (<6.0%) than those from the original method.

Fig. 6 shows a very good relationship among the PAI_{eff} values estimated using the LAI-2200 5R and LAI-2200 4R methods ($R^2 = 0.99$, RMSE = 0.29). A good relationship between the downward DHP Miller and LAI-2200 4R ($R^2 = 0.73$, RMSE = 1.10) can also be observed. There is a weak correspondence between the upward DHP Miller and LAI-2200 4R ($R^2 = 0.56$, RMSE = 0.62). The

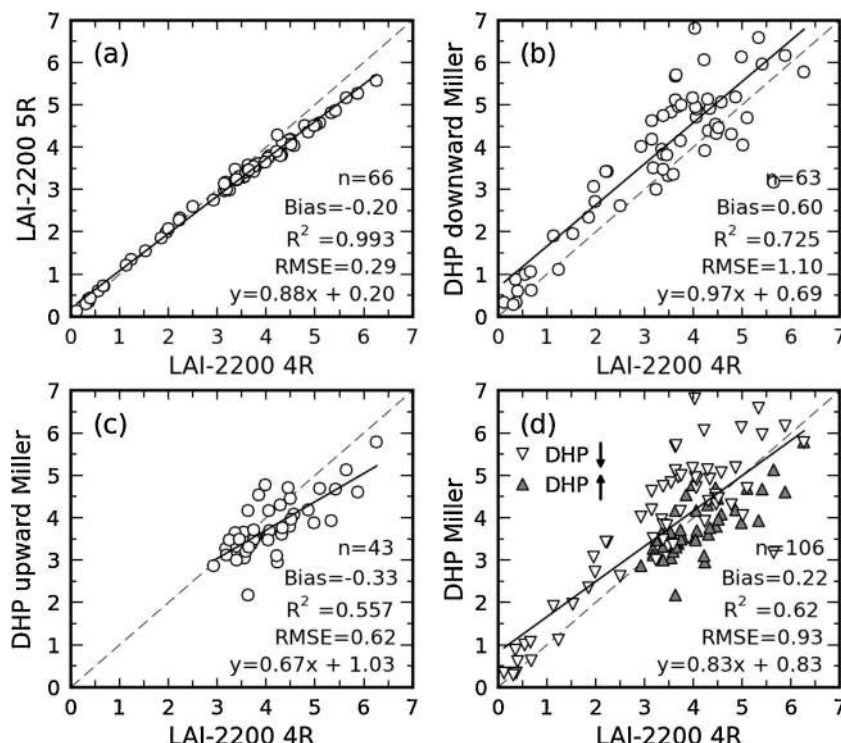


Fig. 6. Comparison of PAI_{eff} retrieved from different optical methods with those from the LAI-2200 4-ring (4R) method. (a) LAI-2200 5-ring (5R), (b) the downward DHP with the Miller's formula (Eq. (3)), (c) the upward DHP with the Miller's formula, and (d) all DHP estimates from the Miller method.

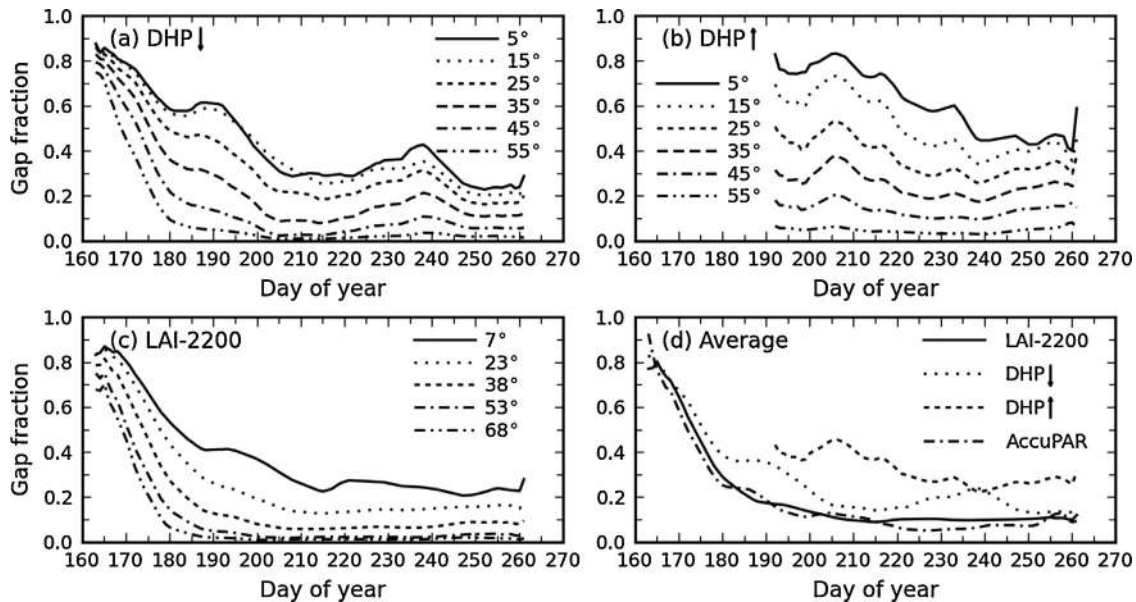


Fig. 7. Seasonal variation of measured gap fractions from the downward DHP (a), the upward DHP (b), and the LAI-2200 (c) methods. Panel (d) shows the angular averages of the LAI-2200, DHP, and AccuPAR estimates.

Table 4

Canopy gap fraction obtained with the indirect optical methods for different periods of the season. The values in the brackets show the relative differences comparing to the LAI-2200 5R (first row).

DOYs	160–190	191–230	231–261	191–261
LAI-2200 5R	0.443	0.117	0.103	0.111
LAI-2200 4R	0.488 (10.2%)	0.143 (22.2%)*	0.125 (21.4%)**	0.135 (21.6%)**
DHP downward	0.529 (19.4%)	0.199 (70.1%)**	0.175 (69.9%)**	0.189 (70.3%)**
DHP upward		0.367 (213.7%)**	0.265 (157.3%)**	0.322 (190.1%)**
AccuPAR	0.427 (-3.6%)	0.101 (-13.7%)	0.081 (-21.4%)**	0.092 (-17.1%)**

* $p < 0.05$.

** $p < 0.01$.

relationships between DHP Miller and LAI-2200 4R (Figs. 6b and c) are similar to those observed between the original DHP and LAI-2200 5R (Fig. 4). Overall, Fig. 6d indicates that the PAI_{eff} values from LAI-2200 4R and DHP Miller are comparable (bias = 0.22, <6.0%).

3.3. Gap fractions

Fig. 7 shows the angular dependence of the measured gap fractions. The optically obtained gap fractions generally decline with the development of canopy leaves (Fig. 7). On average, the gap fractions from LAI-2200 and AccuPAR appear similar, decreasing quickly from about 0.90 at the tiller stage and remaining very low (<0.10) from the early grain filling stage. Note that the gap fraction for AccuPAR is the average of the PAR transmittance (τ in Eq. (8)) within an ESU. The gap fractions estimated by both LAI-2200 and AccuPAR are lower than those obtained by DHP (Fig. 7d), mainly because of the larger viewing angles of the former two sensors. The gap fractions from the downward DHP are higher than those from the LAI-2200 during the two periods of fast LAI change, DOY 180–200 and DOY 225–245, by 0.18 and 0.14, respectively. Gap fractions estimated from the upward DHP are consistently higher (~0.21) than the LAI-2200 and AccuPAR estimates (Table 4).

3.4. Clumping indices

Fig. 8 depicts the seasonal variation in CI derived from DHP as a function of the viewing angle. The CI values estimated from the downward and upward DHPs vary from 0.81 to 0.87 and from 0.69 to 0.78, respectively. The upward DHP shows a similar variation to

the downward DHP, but is systematically lower (~0.08) than the latter over the season (Table 5). On average, CI generally decreases from 0.80 to around 0.68 at the end of July and increases to more than 0.70 from then until the end of the season (Table 5). The rice canopy displays isotropic CI values (0.81) on DOY 171 (June 19). The CI increases with viewing angles before this date when the downward photos were taken with randomly varying azimuth directions. When the DHP images were taken with a fixed azimuth angle, the CI values are found to decrease with the viewing angle ($R^2 = 0.93$ and 0.87 for the downward and upward DHPs) (Figs. 8b and d).

Fig. 9 shows that CI is generally out of phase with LAI, SAI and PAI before DOY 230 (August 17). Both CI and PAI_{eff} values are obtained from the downward DHP photos, and the PAI come from the destructive method. The upward DHP photos were not examined because of the small range of data and the impact of the observation height. A strong negative relationship exists between CI and PAI or PAI_{eff} ($R^2 > 0.80$). The relationships between CI and

Table 5

Clumping index (CI) obtained with the DHP method for different periods of the season. Values in the brackets show the relative differences between the upward and downward CIs. The last row shows the average of the downward and upward DHP values and the standard deviations.

DOYs	160–190	191–230	231–261
DHP downward	0.80	0.72	0.74
DHP upward		0.63 (-12.5%)*	0.66 (-10.8%)*
Average	0.80 ± 0.04	0.68 ± 0.05	0.70 ± 0.04

* $p < 0.01$.

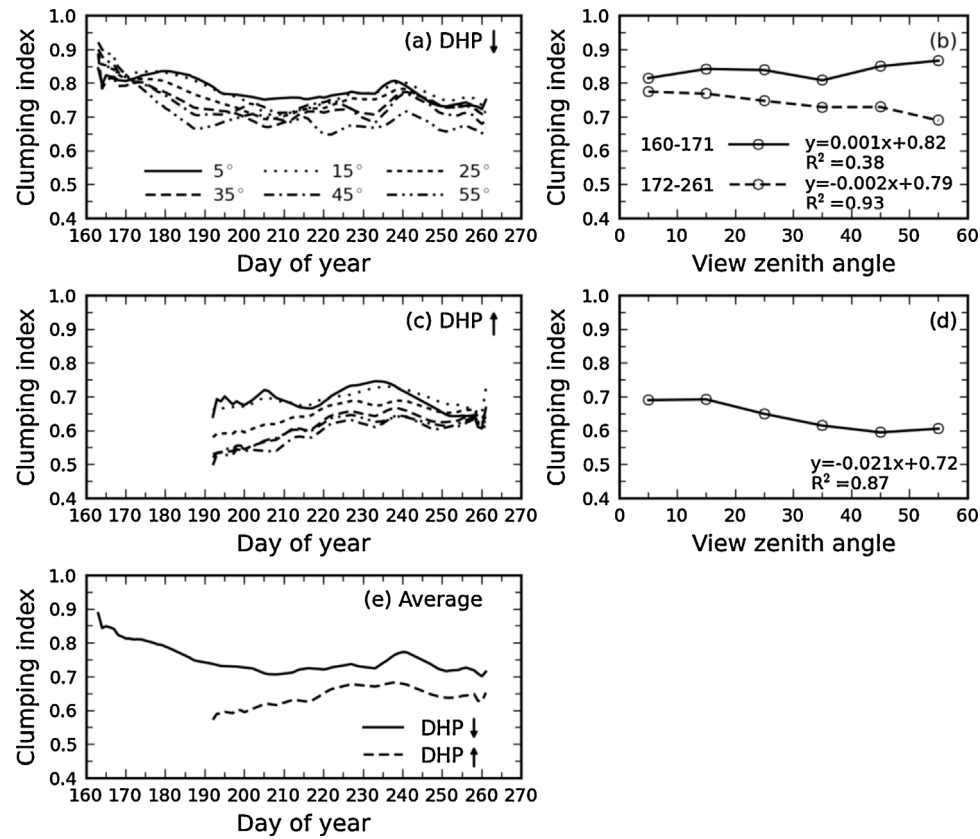


Fig. 8. Seasonal variation of clumping indices (CIs) estimated from the downward (a) and the upward (d) DHP observations. Panels (b) and (d) shows the variation of CIs with view zenith angles. Panel (e) shows the average CIs for both downward and upward DHP observations.

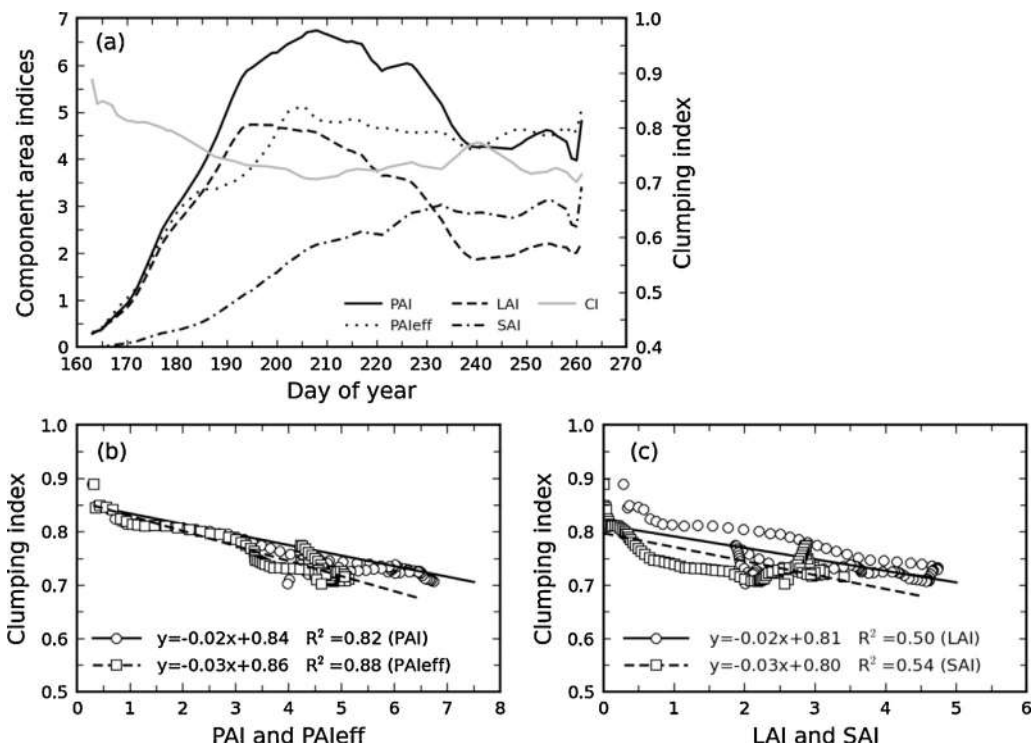


Fig. 9. (a) Seasonal variation of CI and the component area indices; (b) relationships between CI and PAI and PAI_{eff}; (c) relationship between CI and LAI and SAI. CI and PAI_{eff} values are estimated from the downward DHP. PAI, LAI, and SAI values are from the destructive method.

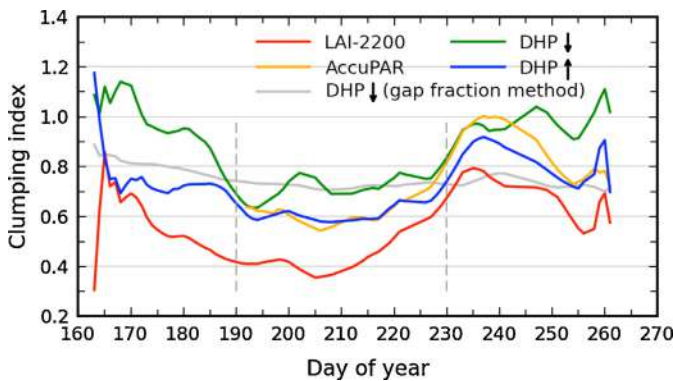


Fig. 10. Seasonal variation of clumping indices estimated as a ratio of the optical PAI_{eff} to the destructive PAI (Eq. (9)). The optical PAI_{eff} values are estimated from LAI-2200, DHP, and AccuPAR, respectively. For comparison, the light gray line shows the CI estimated from DHP using the gap fraction method (Eq. (6)) and Fig. 8e).

LAI and between CI and SAI are moderate ($R^2 = 0.50$ and $R^2 = 0.54$, respectively), indicating that the seasonal variation of CI is related to the development of both leaves and stems.

Fig. 10 depicts the seasonal variation of CIs calculated as a ratio of the optical PAI_{eff} to the destructive PAI (Eq. (9)). The seasonal CI variation is similar to those estimated from DHP using the gap fraction method (Eq. (6), gray line). All CI values decrease with the development of leaves and stems, remain low between DOY 191 (July 9) and 230 (August 17), and increase gradually toward the maturity stage (Table 6). The CI values generally follow the order downward DHP > upward DHP > LAI-2200 > AccuPAR. The upward DHP and LAI-2200 values are similar but differ slightly (<0.10) around DOY 240 (August 27) (Table 6).

3.5. Comparison between optical and destructive PAIs and LAIs

Fig. 11 compares the PAI and LAI values derived from optical methods against the destructive measurements. For DHP, the PAIs were derived by dividing the PAI_{eff} by the corresponding CIs. The PAI values for the LAI-2200 and AccuPAR were derived by dividing PAI_{eff} by the average CI of both DHP views. When the upward DHP CI was not available, the downward DHP CI was used. The destructive, LAI-2200, and DHP PAIs are consistent for most of the season, except after DOY 231 (August 18). During the peak season from DOY 201 to 230, the mean PAI values obtained from LAI-2200 and DHP are nearly identical to the average destructive PAI (Table 7). After the peak season, when the leaves become rolled, the deviations between direct and indirect methods become progressively larger. After DOY 231, the destructive PAI decreases by about 1.80 (−28.6%). However, this amplitude of decrease is not seen by the optical methods. The average LAI-2200 and DHP PAIs decrease by only 0.37 (−5.9%). In general, before DOY 230 (August 17), LAI-2200 provides a very good estimates of destructive PAI (relative errors < 10%), especially when ring 5 is discarded (Table 7). DHP gives even more accurate PAI estimates, with relative errors less than 5%. AccuPAR exhibits the highest underestimation of the destructive PAI by up to 30%.

Table 6

Clumping index (CI) calculated as a ratio of the optical PAI_{eff} and the destructive PAI (Eq. (9)).

DOYs	160–190	191–230	231–261	200	240
LAI-2200	0.75	0.63	0.85	0.61	0.94
DHP downward	0.96	0.74	1.00	0.73	1.00
DHP upward		0.64	0.90	0.60	1.05
AccuPAR	0.55	0.46	0.71	0.41	0.77

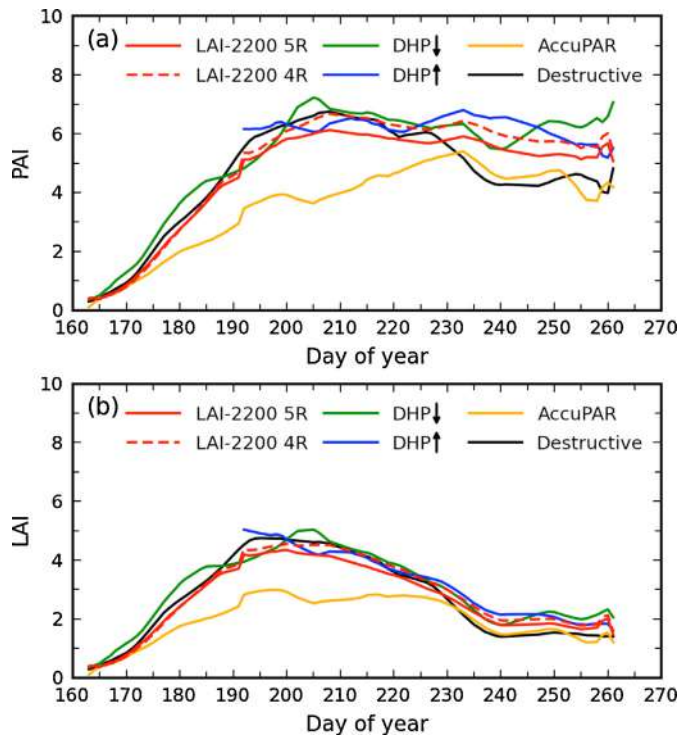


Fig. 11. Seasonal variation of PAIs (a) and LAIs (b) obtained from optical and destructive methods. PAIs are calculated from PAI_{eff} divided by the average CI from the downward and upward DHPs. Optical LAIs are estimated from Eq. (10).

Like PAI, the LAI-2200 and DHP LAI values agree very well with the destructive values before DOY 230, with relative differences less than 10% (Fig. 11b and Table 7). After DOY 231, the relative differences are more than 20%. Comparisons between AccuPAR and the destructive LAIs show more than 30% underestimation before DOY 230 and a very good correspondence after DOY 231 (Table 7). However, the good agreement after DOY 231 may need further verification to ascertain whether it occurs through correct derivation or by artifact.

Overall, LAI-2200 shows a very good relationship with the destructive PAI (Table 8). The relationship is the best between DOY 160 and 230 ($R^2 = 0.84$, RMSE = 0.97). The downward DHP

Table 7

Comparison of the optical PAIs and LAIs over different periods of the season. The values in the brackets show the relative differences comparing to the destructive PAI and LAI.

DOYs	160–200	201–230	231–261
PAI			
Destuctive	3.29	6.31	4.50
LAI-2200 5R	3.00 (−8.8%)	5.89 (−6.7%)*	5.44 (20.9%)*
LAI-2200 4R	3.06 (−7.0%)	6.38 (1.1%)	5.89 (30.9%)*
DHP downward	3.38 (2.7%)	6.63 (5.1%)*	6.14 (36.4%)*
DHP upward		6.30 (0.0%)	6.15 (36.7%)*
AccuPAR	2.08 (−36.8%)*	4.40 (−30.3%)*	4.58 (1.8%)
LAI-2200 5R + DHP	3.51 (6.7%)	6.28 (−0.5%)	5.91 (31.3%)*
LAI-2200 4R + DHP	3.54 (7.6%)	6.44 (2.1%)	6.06 (34.7%)*
LAI			
Destuctive	2.73	3.94	1.58
LAI-2200 5R	2.49 (−8.8%)	3.67 (−6.9%)	1.91 (20.9%)*
LAI-2200 4R	2.53 (−7.3%)	3.97 (−0.8%)	2.07 (31.0%)*
DHP downward	2.82 (3.3%)	4.14 (5.1%)	2.14 (35.4%)
DHP upward		3.91 (−0.8%)	2.16 (36.7%)
AccuPAR	1.73 (−36.6%)*	2.7 (−31.5%)*	1.61 (1.9%)
LAI-2200 5R + DHP	2.89 (5.9%)	3.91 (−0.8%)	2.07 (31.0%)*
LAI-2200 4R + DHP	2.91 (6.7%)	4.01 (1.8%)	2.12 (34.2%)*

* $p < 0.01$.

Table 8

Statistics of the relationship between optical and destructive PAIs/LAIs. The last two rows compare all LAI-2200 and DHP results with the destructive values.

	PAI (160–230)				PAI (160–261)				LAI (160–261)			
	N	Bias	R ²	RMSE	N	Bias	R ²	RMSE	N	Bias	R ²	RMSE
LAI-2200 5R	46	-0.28	0.84	0.97	66	0.07	0.76	1.02	66	-0.05	0.83	0.63
LAI-2200 4R	46	-0.08	0.84	0.98	66	0.36	0.74	1.18	66	0.09	0.81	0.66
DHP downward	45	0.23	0.73	1.30	68	0.72	0.60	1.57	68	0.29	0.72	0.85
DHP upward	27	-0.01	0.16	1.16	49	0.71	0.25	1.46	49	0.24	0.83	0.70
AccuPAR	47	-1.42	0.76	1.89	70	-0.94	0.56	1.66	70	-0.69	0.69	1.16
LAI-2200 5R+DHP	118	-0.02	0.75	1.15	183	0.48	0.62	1.37	183	0.15	0.78	0.74
LAI-2200 4R+DHP	118	0.06	0.76	1.16	183	0.58	0.62	1.42	183	0.20	0.78	0.75

also shows a moderately good relationship ($R^2 = 0.73$, RMSE = 1.30) during the same period. The RMSE values of the upward DHP are comparable to those of the downward DHP. AccuPAR maintains a moderate relationship with the destructive PAI ($R^2 = 0.56$, RMSE = 1.66). However, the underestimation by AccuPAR is clear, especially for the PAI from DOY 160 to 230. With proper corrections for the stem and yellow area ratios, the LAI behaves in a similar fashion to the PAI when compared with the destructive values for the whole season.

4. Discussion

4.1. Intercomparison of optical PAI_{eff} estimates

The downward DHP values are higher than the upward estimates, especially after DOY 200 (Table 2). The difficulties and uncertainties in classifying shadows and mixed pixels may have resulted in the overestimation of PAI_{eff} for the downward DHP. A more rigorous thresholding strategy could decrease the gap fraction and improve the PAI_{eff} estimates. The upward photography is easy for gap identification, but may overestimate the gap fractions and underestimates the PAI_{eff}. In this study, the downward DHP has to be used in the earlier tiller stage before mid-July when rice is lower than 70 cm. After that, the upward DHP is a good alternative to the downward DHP because of the large classification uncertainties of the downward photos. This study has indicated that the PAI and LAI values estimated from the upward DHP agree slightly better with the destructive values than the downward DHP (Table 7). In contrast, other studies for crops have reported that the downward DHP performs better than the upward DHP (Demarez et al., 2008; Garrigues et al., 2008). In practice, the selection of the DHP observation direction is largely dependent upon the complexity of the thresholding process. Potentially, non-green elements can be separated from green foliage using the DHP image, and the yellow area index (YAI) can be estimated from the imagery.

The differences between PAI_{eff} and PAI values estimated from LAI-2200 and DHP are less than 0.80 (Tables 2 and 7). Other studies have also indicated that the differences in the optical measurements are usually less than 1.0 for all biome types (Asner et al., 2003; Chen et al., 2006; Coops et al., 2004; Garrigues et al., 2008). Compared to the PAI_{eff} values estimated by LAI-2200, the relative differences are within 20% and 5%, respectively, for the downward and upward DHP estimates, from DOY 191 to 230 (Table 2). Similarly, the larger differences for the downward DHP can be mainly attributed to the difficulties in image classification.

The differences between PAI_{eff} estimated from the LAI-2200 4R and from the DHP with the Miller method (Fig. 6) represent the differences in the measured gap fractions (Table 3) and in the retrieval algorithms. LAI-2200 4R calculates PAI_{eff} from Eq. (4), while the DHP Miller uses an integral form of Eq. (3). Moreover, the DHP PAI_{eff} is calculated from the gap fraction averaged over the whole ESU. For the LAI-2200, the PAI_{eff} is calculated as the average of four individual PAI_{eff} values within an ESU.

LAI-2200 has adjusted the weighting factors assigned to different rings in order to minimize the contribution of diffuse light in ring 5 from multiple scattering (LI-COR, 2010). The LAI-2200 uses only the discrete bands actually viewed by the rings, whereas the original LAI-2000 assigned ring weights based on the entire 0°–90° span (Appendix A). The consistency between LAI-2200 and DHP for the PAI_{eff} estimation (Fig. 3) and the accurate PAI estimates obtained by LAI-2200 (Table 7) illustrate the improvement of the new weight configurations. The PAI_{eff} retrieved from LAI-2200 4R is about 8.0% higher than the values from 5R (Table 2). Other studies have reported more than 11–20% increases in the estimated PAI_{eff} when LAI-2000 ring 5 is excluded (Chen, 1996; Chen et al., 2006; Cutini et al., 1998; Stroppiana et al., 2006). The smaller differences between LAI-2200 4R and 5R retrievals confirm the improvement of the LAI-2200 over the earlier model and the likely residual multiple scattering effects using four rings.

AccuPAR is known to give underestimates during clear days due to direct sunlight, especially in canopies with large gaps (Decagon Devices, 2004). This study has found an average 30% underestimation under the diffuse light conditions (Table 2). Underestimation by AccuPAR has been noticed in other similar studies (Garrigues et al., 2008; Jonckheere et al., 2004). For example, Garrigues et al. (2008) reported that AccuPAR underestimates DHP by about 1.0 for crops. The lower AccuPAR estimation may be attributed to the theoretical basis of its algorithm and its wide viewing angles. AccuPAR makes observations at the full PAR band and all zenith angles which may include diffuse light contributions from multiple scattering (Jensen et al., 2011), which may lead to systematic underestimation of the PAI_{eff} (Chen et al., 2006, 1997). Further investigation is therefore warranted on the issues related to the AccuPAR underestimation.

4.2. Retrieval of gap fractions

The differences between downward and upward DHPs are mainly related to the distance between the camera and the canopy top. The height of rice influences the distance from canopy top to camera, which affects the gap fraction measurement. The upward DHPs were taken when the rice was higher than 70 cm (after July 10). The small distance from camera to canopy top results in gap fractions retrieved from the upward images about 60% larger than retrieved from the downward images (Table 4). This leads to lower PAI_{eff} values from the upward DHP than from the downward DHP, especially in the early stage between DOY 201 and 230 (Fig. 3 and Table 2). The gap fractions obtained from the downward DHP are higher than those from LAI-2200 around DOY 190 and 240, a result that can be attributed to the classification uncertainties and the DHP overexposure. The level of difference is similar to the gap differences observed between DHP and TRAC (Leblanc et al., 2005). For the upward DHP, the gap fractions are consistently higher than those from the LAI-2200 due to the higher DHP observational height.

Similar PAI_{eff} values are obtained from both LAI-2200 and DHP even with the differences in the measured gap fractions (Table 2).

The similarity between the PAI_{eff} values may be partly attributed to the CAN_EYE algorithms which use the PAI_{eff} estimated at 57° as constraints (Eq. (8) in Weiss and Baret, 2010) and are therefore sensitive to observations round 57°. The observed gap fractions at 57° from DHP and LAI-2200 are nearly the same (Fig. 7). Note that the modeled gap fractions from both instruments are similar (Fang et al., 2014). However, the 57° observations are near the DHP cutoff angle (60°), which may inevitably lead to higher uncertainties for the PAI_{eff} estimates close to the edges.

4.3. Clumping index (CI)

The CI values estimated by the upward DHP are slightly less (<0.10) than those from the downward DHP (Table 5). The higher CI values (less clumping) from the downward DHP may be related to the higher portion of leaves and ears, which are more randomly distributed in its field of view. In the field experiments, the upward camera was usually positioned in the middle of the rows, which provides a distinct contrast between canopy and sky, but may have led to a lower clumping index.

The seasonal dynamics of CI are consistent with other findings that CI tends to decrease with the canopy development and crown thickening (Pisek et al., 2013; Ryu et al., 2010a). Before DOY 190 (July 8), the distribution of leaves is more random and the gradual decrease of CI may be attributed to the stem growth. Between DOY 191 and 230, the combined effects of stems and ears may intensify the clumping effect. Between DOY 231 and 250, the intervention of rice ears and the leaf bending may have improved the randomness of the effective components observed by the optical instruments. After DOY 251, the leaf rolling and the exposure of stems caused by winds correspond to an increase in leaf clumping during the late stage (Fig. 8). The distinct seasonal dynamics of the CI values should be considered in the retrieval of time series LAI and PAI from remotely sensed data (Fang et al., 2013).

During the first 10 days, the downward DHP images were taken with random azimuth angles and the CI values have been consistently higher than those estimated with a fixed azimuth angle (Fig. 8b). The azimuthal variation of the gap fraction has been normalized during the random sampling process. A fixed azimuth angle to the row direction was used after DOY 171 and CI is found to decrease with viewing angle ($R^2 > 0.87$). This angular dependence of CI is mainly attributed to the gap size distribution (Chen, 1996; Kucharik et al., 1999; Ryu et al., 2010b). For rice canopies, large inter-row gaps (high clumping) are commonly visible at high viewing angles for large LAI values because of the regularly spaced canopy crowns. This trend has also been shown for the heterogeneous savanna ecosystem (Ryu et al., 2010b). The erectophile type of rice leaves and stems also contribute to the CI variation. The fields are covered with only young sparse leaves (LAI < 1.0) before DOY 171, which appear denser (smaller gaps) at larger viewing angles. Afterwards, the stem area gradually increases and may have led to a decrease of CI with the viewing angle.

The strong CI-PAI and CI-PAI_{eff} relationships revealed in this study (Fig. 9) provide a simple method to estimate seasonal CI from remotely sensed data. This function can be incorporated into land surface models to help parameterize the vegetation clumping properties (Chen et al., 2012; Ni-Meister and Gao, 2011; Pinty et al., 2006). Indeed, the relationship is expected to be biome and site specific. The negative relationship between CI and PAI or PAI_{eff} can be explained by the row effects of the rice canopies. A similar phenomenon has been reported for invasive weeds, which was also related to the spatial heterogeneity of the vegetation (Ryu et al., 2010a). Some studies for evergreen needleleaf forests have suggested that CI declines exponentially with PAI (Chen, 1996; Sampson and Smith, 1993), while others have reported that CI increases with PAI_{eff} for deciduous broadleaf forests (Ryu et al.,

2010a). Further studies are therefore necessary to provide a better understanding the relationship between CI and PAI and its seasonal dynamics.

In this study, CI was also determined as a ratio of the optical PAI_{eff} and the destructive PAI (Table 5). The ratio method needs to be noted because of the multiple scattering effect on the PAI_{eff} estimation from the LAI-2200 instrument (Chen et al., 1997). The results of this study show that the CI values from both optical (Eq. (6)) and ratioing (Eq. (9)) methods agree very well during the peak growing season (DOY 191–230) (Tables 5 and 6). These results confirm the feasibility of CI estimation using the ratio method (Duthoit et al., 2008; Ryu et al., 2010b). During the peak growing period, the high PAI_{eff} (>3.5) and the very low gap fractions (Fig. 7) indicate that the multiple-scattering effect may have been suppressed to some extent with the new LAI-2200 configuration. During the early (before DOY 190) and the late seasons (after DOY 231), the ratioing CI values are about 0.15–0.30 (or 20–40%) higher than the optical CI estimates. This discrepancy may be attributed to the uncertainties in the gap fraction and the PAI_{eff} and PAI estimates (Sections 4.1 and 4.2).

4.4. Inter-comparison of PAIs and LAIs

The optical PAI values agree better with the destructive PAI values before DOY 230 than when measurements from all dates are considered (Fig. 11a). As the leaves become senescent after DOY 231, both destructive and optical methods show a loss of sensitivity or an inability to detect changes in LAI and PAI, with relative errors > 20% (Table 7). With more senescent leaves, the destructive method significantly underestimates the leaf surface area because of the rolling of yellow leaves. The optical measurements also suffer from the leaf rolling and bending. The large scatters after DOY 230 in Fig. 11a are indications of all the above effects.

The good correspondence between the optical and destructive PAIs/LAIs in Fig. 11 suggests that the DHP derived CI is adequate for the transformation of the PAI_{eff} derived from LAI-2200 and DHP into PAI. This also shows the effectiveness of using the stem and yellow area ratios to derive LAI from optically measured PAI_{eff}. These ratios and the LAI estimation method (Eq. (10)) may be extended to other areas and to other crop types. Indeed, the clumping correction can be difficult in field optical measurements and it is not always possible to exclude the influence of stems, whereas the actual LAI definition includes only leaves.

The results from the comparison of the destructive and optical LAI measurements are comparable to other similar studies. The high correlation between LAI-2200 estimates and destructive PAI measurements ($R^2 > 0.84$) has also been shown by other studies (Stroppiana et al., 2006). In general, the optical method provides a convenient and sufficiently accurate method to estimate PAI. LAI-2200 provides the most efficient approach for field PAI estimation in paddy rice fields ($R^2 > 0.83$, RMSE < 1.00) with relative errors < 10% (Table 7). The DHP method generally gives highly accurate estimates of the destructive PAI, with a slight overestimation of no more than 5% (before DOY 230). This level of nearly perfect correspondence is in clear contrast to the level of error (~15%) reported previously by Jonckheere et al. (2004). In general, DHP offers a good alternative to LAI-2200 and is particularly promising for investigating the development of rice plants, by itself or in association with LAI-2200.

4.5. Uncertainties and future prospects

Uncertainties may arise in several ways, such as the algorithm theoretical basis, retrieval uncertainties, measurement issues, and other random errors. The uncertainty in the direct method may

arise from the limited number of destructive samples. LAI-2200 assumes black leaves using a blue band (320–490 nm) within which leaves absorb the most radiation. However, leaves are not completely black. They transmit and reflect light even in the blue band so that there is some residual transmission through the leaves (Gates et al., 1965; Kobayashi et al., 2013; Welles and Norman, 1991). The illumination conditions might change from measurement to measurement, which would inevitably affect the comparison of multiple observations. Light might be expected to diminish between upper and lower measurements for both LAI-2200 and AccuPAR. The situation is aggravated when plants grow denser and taller because illumination becomes weak deep inside the canopy. The accuracy of LAI estimation from DHP is dependent on the accuracy of a classification procedure which involves subjective determination of plant pixels and gaps. This procedure may be difficult under dense canopies due to the similarity among plant pixels, gaps, and their mixture, especially for the downward view. Weak illumination conditions increase the uncertainty of gap fraction quantification in areas covered by shading and shadows.

The averaging methods within an ESU are different for LAI-2200 and DHP. LAI-2200 calculates the PAI from each point and then averages these values on the ESU scale, while DHP calculates the average gap fraction within an ESU first and then retrieves PAI from the gap fraction. For seasonal continuous measurement, it is difficult to maintain a consistent observation protocol under variable weather and field conditions. Occasional system failures occur as a result of power loss or water drops on the glass windows of optical instruments. For LAI-2200, different view caps have to be used in case of missing caps in the field. For the upward DHP, the lower leaves of crop canopies can be very close to the camera lens. The inclement weather in the late August bent down stems in the rice fields and considerably hampered field measurements.

It is apparent that field LAI measurements need to be performed at high temporal resolutions, preferably for an entire growing season, to obtain a clear characterization of the LAI temporal profile. Such measurements have become very useful in the validation of LAI and other land products as time series studies have become more and more important (Camacho et al., 2013; Claverie et al., 2013; Fang et al., 2012a; Heiskanen et al., 2012; Xiao et al., 2014). On the other hand, continuous seasonal measurements are labor and cost intensive. Some researchers have suggested the use of normal digital cameras for continuous LAI monitoring because DHP is sensitive to photographic exposure (Chianucci and Cutini, 2013; Ryu et al., 2012; Sakamoto et al., 2012). Recently, several automatic instruments, e.g., the PASTIS-57 (Baret et al., 2010), the LAINet (Qu et al., 2014), and the LED senors (Ryu et al., 2014), have been tested experimentally to estimate the seasonal PAI with a high temporal sampling rate. These instruments deserve further investigation for crop LAI measurement.

5. Conclusion

This paper compares both destructive and optical field LAI measurement methods over paddy rice fields in NE China. Seasonal variations of rice area indices for green leaves, yellow leaves, stems, and total plants were obtained from the destructive method. LAI-2200 shows improvement over the earlier LAI-2000, with more reasonable weights for ring 5, and has thus decreased the multiple scattering effects at high zenith angles. Both LAI-2200 and DHP generate consistent effective PAI (PAI_{eff}) estimates during the season ($R^2 = 0.76$, RMSE = 0.97). However, AccuPAR systematically underestimates the PAI_{eff} values from LAI-2200 and DHP.

The measured gap fractions from LAI-2200 and AccuPAR agree well over the season. The downward DHP measurements are usually higher, especially during periods of fast LAI change, as a result of the photo quality and the classification uncertainties. The greater observational heights for the upward DHP leads to higher (~0.21) gap fraction observations than those from LAI-2200.

The canopy CI can be derived from DHP with a fixed viewing azimuth direction. The CI values follow a clear seasonal pattern, decreasing with the plant growth and increasing during the late senescent stage. The CI values range between 0.63 and 0.74 during the peak growing period between DOY 191–230, similar to the CIs derived with the $\text{PAI}_{\text{eff}}/\text{PAI}$ method, which indicates that the ratio method can be used to acquire landscape CI during the plateau stage. The CI values generally decrease with the increasing angles for rice crops. The strong linear CI-PAI and CI- PAI_{eff} relationships suggest that the seasonal dynamics of CI can be estimated as a function of PAI or PAI_{eff} .

Compared to the destructive values, both LAI-2200 and DHP are able to generate very accurate PAI and LAI estimates, with relative errors less than 10% and 5%, respectively, before DOY 230 (August 17). Omitting ring 5 for LAI-2200 results in nearly perfect PAI estimation, indicating the effectiveness of the new weighting factors for the instrument. AccuPAR produces the greatest underestimation of the destructive PAI and LAI, by around 30%. Both PAI and LAI estimates during the senescent period after DOY 231 are unreliable, with relative errors >20%, because of the huge uncertainties in both destructive and optical methods.

LAI-2200 avoids the subjective classification procedure and offers an easy way to derive PAI_{eff} . The downward DHP is preferable during the early growing season when rice is lower than 70 cm. After that, the upward DHP is a good alternative to the downward DHP because of the larger classification uncertainties of the latter. It is recommended to combine both LAI-2200 and DHP in field PAI_{eff} and PAI estimation. The data obtained from this study provide a benchmark for understanding the structure and seasonal variation of rice LAI at landscape scales and should aid in the Land Product Validation (LPV) studies (<http://lpvs.gsfc.nasa.gov/>) that are currently being undertaken by the community.

Acknowledgments

This study was supported by the National Natural Science Foundation of China (41171333) and the Hundred Talent Program of the Chinese Academy of Sciences. We would like to thank the interns who attended the field work at various stages, and the farmers for allowing us to make use of their fields for in situ measurements.

Appendix A.

The weighting factors for different LAI-2200 and LAI-2000 rings. The LAI-2200 only uses the discrete bands actually viewed by the rings, while the LAI-2000 assigns ring weights based on the entire interval between 0° and 90°. Weighting factors using all five rings (5R) and the inner four rings (4R) are shown.

Ring #	Ring center	Nominal range	LAI-2200		LAI-2000	
			5R ^a	4R ^b	5R ^c	4R ^b
1	7°	0.0–12.3°	0.041	0.062	0.034	0.067
2	23°	16.7–28.6°	0.131	0.198	0.104	0.202
3	38°	32.4–43.4°	0.201	0.302	0.160	0.318
4	53°	47.3–58.1°	0.290	0.438	0.218	0.413
5	68°	62.3–74.1°	0.337		0.494	

^a LI-COR (2010).

^b Derived in this study.

^c LI-COR (1991).

Appendix B. Supplementary data

Supplementary data associated with this article can be found, in the online version, at <http://dx.doi.org/10.1016/j.agrformet.2014.08.005>.

References

- Asner, G.P., Scurlock, J.M.O., Hicke, J.A., 2003. Global synthesis of leaf area index observations: implications for ecological and remote sensing studies. *Glob. Ecol. Biogeogr.* 12, 191–205.
- Baret, F., de Solan, B., Lopez-Lozano, R., Ma, K., Weiss, M., 2010. LAI estimates of row crops from downward looking digital photos taken perpendicular to rows at 57° zenith angle: theoretical considerations based on 3D architecture models and application to wheat crops. *Agric. For. Meteorol.* 150 (11), 1393–1401.
- Bonan, G.B., Levis, S., 2006. Evaluating aspects of the community land and atmosphere models (CLM3 and CAM3) using a dynamic global vegetation model. *J. Clim.* 19 (11), 2290–2301.
- Camacho, F., Cernicharo, J., Lacaze, R., Baret, F., Weiss, M., 2013. GEOV1: LAI, FAPAR essential climate variables and FCOVER global time series capitalizing over existing products. Part 2: validation and intercomparison with reference products. *Remote Sens. Environ.* 137, 310–329.
- Chen, J.M., 1996. Optically based methods for measuring seasonal variation of leaf area index in boreal conifer stands. *Agric. For. Meteorol.* 80 (2–4), 135–163.
- Chen, J.M., Black, T.A., 1992. Defining leaf area index for non-flat leaves. *Plant Cell Environ.* 15 (4), 421–429.
- Chen, J.M., Cihlar, J., 1995. Plant canopy gap-size analysis theory for improving optical measurements of leaf-area index. *Appl. Opt.* 34, 6211–6222.
- Chen, J.M., et al., 2006. Leaf area index measurements at Fluxnet-Canada forest sites. *Agric. For. Meteorol.* 140 (1–4), 257–268.
- Chen, J.M., et al., 2012. Effects of foliage clumping on the estimation of global terrestrial gross primary productivity. *Glob. Biogeochem. Cycles* 26 (1), <http://dx.doi.org/10.1029/2010gb003996>.
- Chen, J.M., Rich, P.M., Gower, S.T., Norman, J.M., Plummer, S., 1997. Leaf area index of boreal forests: theory, techniques and measurements. *J. Geophys. Res.* 102, 29429–29443.
- Chianucci, F., Cutini, A., 2013. Estimation of canopy properties in deciduous forests with digital hemispherical and cover photography. *Agric. For. Meteorol.* 168 (0), 130–139.
- Claverie, M., et al., 2013. Validation of coarse spatial resolution LAI and FAPAR time series over cropland in southwest France. *Remote Sens. Environ.* 139 (0), 216–230.
- Coops, N.C., Smith, M.L., Jacobsen, K.L., Martin, M., Ollinger, S., 2004. Estimation of plant and leaf area index using three techniques in a mature native eucalypt canopy. *Austral Ecol.* 29, 332–341.
- Cutini, A., Matteucci, G., Mugnozza, G.S., 1998. Estimation of leaf area index with the Li-Cor LAI 2000 in deciduous forests. *For. Ecol. Manage.* 105 (1–3), 55–65.
- Deblonde, G., Penner, M., Royer, A., 1994. Measuring leaf area index with the LI-COR LAI-2000 in pine stands. *Ecology* 75, 1507–1511.
- Decagon Devices, 2004. AccuPAR PAR/LAI Ceptometer (model LP-80) Operator's Manual Version 1.2, Pullman, WA 99162, USA.
- Demarez, V., Duthoit, S., Baret, F., Weiss, M., Dedieu, G., 2008. Estimation of leaf area and clumping indexes of crops with hemispherical photographs. *Agric. For. Meteorol.* 148 (4), 644–655.
- Duthoit, S., Demarez, V., Gastello-Etchegorry, J.-P., Martin, E., Roujean, J.-L., 2008. Assessing the effects of the clumping phenomenon on BRDF of a maize crop based on 3D numerical scenes using DART model. *Agric. For. Meteorol.* 148 (8–9), 1341–1352.
- Fang, H., et al., 2013. Characterization and intercomparison of global moderate resolution leaf area index (LAI) products: analysis of climatologies and theoretical uncertainties. *J. Geophys. Res. Biogeosci.* 118 (2), 529–548.
- Fang, H., Li, W., Wei, S., Sun, T., Jiang, C., 2014. Paddy Rice Experiment in the Sanjiang Plain (PRESP): Field Measurement Report. Institute of Geographic Sciences and Natural Resources Research, Chinese Academy of Sciences http://www.lreis.ac.cn/upload/article/Fang2014_PRESP.pdf
- Fang, H., Wei, S., Liang, S., 2012a. Validation of MODIS and CYCLOPES LAI products using global field measurement data. *Remote Sens. Environ.* 119, 43–54.
- Fang, H., Xiao, Z., Qu, Y., Song, J., 2012b. Leaf area index. In: Liang, S., Li, X., Wang, J. (Eds.), *Advanced Remote Sensing: Terrestrial Information Extraction and Applications*. Academic Press, Boston/Tokyo, pp. 347–381.
- Garrigues, S., et al., 2008. Intercomparison and sensitivity analysis of leaf area index retrievals from LAI-2000, AccuPAR, and digital hemispherical photography over croplands. *Agric. For. Meteorol.* 148, 1193–1209.
- Gates, D.M., Keegan, H.J., Schleter, J.C., Weidner, V.R., 1965. Spectral properties of plants. *Appl. Opt.* 4 (1), 11–20.
- GCOS, 2011. Systematic Observation Requirements for Satellite-Based Products for Climate, 2011 Update, Supplemental Details to the Satellite-Based Component of the Implementation Plan for the Global Observing System for Climate in Support of the UNFCCC (2010 Update). <http://www.wmo.int/pages/prog/gcos/Publications/gcos-154.pdf>
- Gobron, N., Verstraete, M.M., 2009. Assessment of the Status of the Development of the Standards for the Terrestrial Essential Climate Variables: Leaf Area Index (LAI). Global Terrestrial Observing System, Rome <http://www.fao.org/gtos/doc/ECVs/T10/T10.pdf>
- Heiskanen, J., et al., 2012. Seasonal variation in MODIS LAI for a boreal forest area in Finland. *Remote Sens. Environ.* 126 (0), 104–115.
- Jensen, J.R.R., Humes, K.S., Hudak, A.T., Vierling, L.A., Delmelle, E., 2011. Evaluation of the MODIS LAI product using independent lidar-derived LAI: a case study in mixed conifer forest. *Remote Sens. Environ.* 115 (2), 3625–3639.
- Jonckheere, I., et al., 2004. Review of methods for in situ leaf area index determination. Part I. Theories, sensors and hemispherical photography. *Agric. For. Meteorol.* 121 (1–2), 19–35.
- Kobayashi, H., Ryu, Y., Baldocchi, D.D., Welles, J.M., Norman, J.M., 2013. On the correct estimation of gap fraction: how to remove scattered radiation in gap fraction measurements? *Agric. For. Meteorol.* 174–175, 170–183.
- Kucharik, C.J., Norman, J.M., Gower, S.T., 1999. Characterization of radiation regimes in non-random forest canopies: theory, measurements, and simplified modeling approach. *Trees Physiol.* 19, 695–706.
- Lafont, S., et al., 2012. Modelling LAI, surface water and carbon fluxes at high-resolution over France: comparison of ISBA-A-gs and ORCHIDEE. *Biogeosciences* 9 (1), 439–456.
- Lang, A.R.G., 1987. Simplified estimate of leaf area index from transmittance of the sun's beam. *Agric. For. Meteorol.* 41, 179–186.
- Lang, A.R.G., 1991. Application of some of Cauchy's theorems to estimation of surface areas of leaves, needles and branches of plants, and light transmittance. *Agric. For. Meteorol.* 55 (3–4), 191–212.
- Lang, A.R.G., McMurtrie, R.E., Benson, M.L., 1991. Validity of surface area indices of *Pinus radiata* estimated from transmittance of the sun's beam. *Agric. For. Meteorol.* 57 (1–3), 157–170.
- Lang, A.R.G., Xiang, Y., 1986. Estimation of leaf area index from transmission of direct sunlight in discontinuous canopies. *Agric. For. Meteorol.* 37 (3), 229–243.
- Leblanc, S.G., Chen, J.M., Fernandes, R., Deering, D.W., Conley, A., 2005. Methodology comparison for canopy structure parameters extraction from digital hemispherical photography in boreal forests. *Agric. For. Meteorol.* 129 (3–4), 187–297.
- LI-COR Inc., 1991. LAI-2000 Plant Canopy Analyzer: Instruction Manual. LI-COR Inc., Lincoln, Nebraska 68504, USA.
- LI-COR Inc., 2010. LAI-2200 Plant Canopy Analyzer: Instruction Manual. LI-COR Inc., Lincoln, Nebraska 68504, USA.
- Miller, J.B., 1967. A formula for average foliage density. *Aust. J. Bot.* 15, 141–144.
- Morisette, J.T., et al., 2006. Validation of global moderate-resolution LAI products: a framework proposed within the CEOS land product validation subgroup. *IEEE Trans. Geosci. Remote Sens.* 44 (7), 1804–1817.
- Ni-Meister, W., Gao, H.L., 2011. Assessing the impacts of vegetation heterogeneity on energy fluxes and snowmelt in boreal forests. *J. Plant Ecol.* 4 (1–2), 37–47.
- Nilson, T., 1971. A theoretical analysis of the frequency of gaps in plant stands. *Agric. Meteorol.* 8, 25–38.
- Norman, J.M., Welles, J.M., 1983. Radiative transfer in an array of canopies. *Agron. J.* 75, 81–488.
- Pinty, B., et al., 2006. Simplifying the interaction of land surfaces with radiation for relating remote sensing products to climate models. *J. Geophys. Res.* 111 (D02116), <http://dx.doi.org/10.1029/2005JD005952>.
- Pisek, J., et al., 2013. Retrieving vegetation clumping index from Multi-angle Imaging SpectroRadiometer (MISR) data at 275 m resolution. *Remote Sens. Environ.* 138 (0), 126–133.
- Qu, Y., Zhu, Y., Han, W., Wang, J., Ma, M., 2014. Crop leaf area index observations with a wireless sensor network and its potential for validating remote sensing products. *IEEE J. Sel. Top. Appl. Earth Observ. Remote Sens.* 7 (2), 431–444.
- Ryu, Y., et al., 2010a. On the correct estimation of effective leaf area index: does it reveal information on clumping effects? *Agric. For. Meteorol.* 150 (3), 463–472.
- Ryu, Y., et al., 2010b. How to quantify tree leaf area index in an open savanna ecosystem: a multi-instrument and multi-model approach. *Agric. For. Meteorol.* 150, 63–76.
- Ryu, Y., et al., 2012. Continuous observation of tree leaf area index at ecosystem scale using upward-pointing digital cameras. *Remote Sens. Environ.* 126 (0), 116–125.
- Ryu, Y., Lee, G., Jeon, S., Song, Y., Kimm, H., 2014. Monitoring multi-layer canopy spring phenology of temperate deciduous and evergreen forests using low-cost spectral sensors. *Remote Sensing of Environment* 149, 227–238.
- Sakamoto, T., et al., 2012. An alternative method using digital cameras for continuous monitoring of crop status. *Agric. For. Meteorol.* 154–155 (0), 113–126.
- Sampson, D.A., Smith, F.W., 1993. Influence of canopy architecture on light penetration in lodgepole pine (*Pinus contorta* var. *latifolia*) forests. *Agric. For. Meteorol.* 64 (1–2), 63–79.
- Song, C., Xu, X., Tian, H., Wang, Y., 2009. Ecosystem–atmosphere exchange of CH₄ and N₂O and ecosystem respiration in wetlands in the Sanjiang Plain, Northeastern China. *Glob. Chang. Biol.* 15 (3), 692–705.
- Stenberg, P., 2006. A note on the G-function for needle leaf canopies. *Agric. For. Meteorol.* 136 (1–2), 76–79.
- Stroppiana, D., Boschetti, M., Confalonieri, R., Bocchi, S., Brivio, P.A., 2006. Evaluation of LAI-2000 for leaf area index monitoring in paddy rice. *Field Crops Res.* 99 (2–3), 167–170.
- Tian, Y., et al., 2004. Comparison of seasonal and spatial variations of leaf area index and fraction of absorbed photosynthetically active radiation from Moderate Resolution Imaging Spectroradiometer (MODIS) and common land model. *J. Geophys. Res.* 109 (D01103), <http://dx.doi.org/10.1029/2003JD003777>.
- Weiss, M., Baret, F., 2010. CAN-EYE V6.1 User Manual. <http://www6.paca.inra.fr/can-eye/Documentation-Publications/Documentation>

- Weiss, M., Baret, F., Myneni, R.B., Pragnere, A., Knyazikhin, Y., 2000. Investigation of a model inversion technique to estimate canopy biophysical variables from spectral and directional reflectance data. *Agronomie* 20 (1), 3–22.
- Weiss, M., Baret, F., Smith, G.J., Jonckheere, I., Coppin, P., 2004. Review of methods for in situ leaf area index (LAI) determination. Part II. Estimation of LAI, errors and sampling. *Agric. For. Meteorol.* 121 (1–2), 37–53.
- Welles, J.M., Norman, J.M., 1991. Instrument for indirect measurement of canopy architecture. *Agron. J.* 83 (5), 818–825.
- Xiao, Z., et al., 2014. Use of general regression neural networks for generating the GLASS leaf area index product from time-series MODIS surface reflectance. *IEEE Trans. Geosci. Remote Sens.* 52 (1), 209–223.
- Yang, W., Hao, F., Cheng, H., Lin, C., Ouyang, W., 2013. Phosphorus fractions and availability in an albic bleached meadow soil. *Agron. J.* 105 (5), 1451–1457.